Hindawi
Shock and Vibration
Volume 2019, Article ID 9407520, 12 pages
https://doi.org/10.1155/2019/9407520

Research Article

Resonance Suppression for Hydraulic Servo Shaking Table Based on Adaptive Notch Filter

Jianjun Yao, Zhenshuai Wan, Yue Zhao, Jie Yu, Chen Qian, and Yu Fu

College of Mechanical and Electrical Engineering, Harbin Engineering University, Harbin 150001, China

Correspondence should be addressed to Zhenshuai Wan; 18242311944@163.com

Received 25 January 2019; Revised 27 April 2019; Accepted 8 May 2019; Published 21 May 2019

Academic Editor: Mario Terzo

In dynamic structure test, the specimen of hydraulic servo shaking table contains not only inertia load but also elastic load. The specimen herein is simplified as a spring-mass-damping system, and the mathematical model of the hydraulic servo shaking table is established by theoretical analysis. The coupling between specimen's elastic load and shaking table itself produces resonance phenomenon in the required bandwidth when the elastic load is not negligible, which deteriorates the system's dynamic performance and even leads to the instability of the control system. Also, the time-varying resonance frequency further aggravates the control performance of the system in the shaking test. In this paper, an adaptive notch filter based on least mean square (LMS) error principle is employed to identify the resonance frequencies online and real-time adjust the parameters of the notch filter. Simulation and experiment results show the effectiveness of frequency identification and resonance mode suppression. Compared with the existing resonance suppression scheme, the proposed method can suppress the appeared resonance mode adaptively.

1. Introduction

Considering the repeatability, safety, and cost, the mechanical properties of structure and components are usually tested using dynamic laboratory test rather than field test [1–4]. As one of the most important dynamic structure test devices, shaking table is widely used in industrial fields including seismic simulation, aerospace, and infrastructure [5–8]. Compared with mechanical shaker and electrodynamic shaker, hydraulic servo shaking table has such merits as high power to weight ratio, load stiffness, response speed, and control precision, and these features make it invaluable in the dynamic structure test [9, 10]. In previous studies, the specimen of hydraulic servo shaking table is often considered as inertial load, in other words, without consideration of the effect of elastic load. However, the elastic load of the specimen in the dynamic structure test is too big to be ignored [11]. The coupling between the specimen's elastic load and shaking table itself produces resonance phenomenon in the required bandwidth when the elastic load is not negligible, which reduces the system's dynamic performance and even leads to the instability of the control system. Increased accuracy in dynamic structure test requires a high bandwidth. However, the bandwidth cannot be increased arbitrarily due to the appeared resonance modes. Moreover, the resonance frequency can vary during the operation of hydraulic servo shaking table because of various factors such as fabrication errors, hydraulic cylinder leakage, and hydraulic fluid compressibility [12]. This leads to that the conventional control method is difficult to achieve exact tracking response and may result in damage to the specimen.

Several methods have been studied to solve the resonance problem [13]. Schmidt and Rehm adopted fast Fourier transform (FFT) to measure resonance frequency and calculate antiresonant frequency of a dual inertia spring system [14]. Wang et al. used an adaptive notch filter with a FFT analyzer based on a sorting algorithm and nonlinear model predictive controller to suppress the low-order torsional vibration and compensate for the dynamic control performance of a helicopter system, respectively [15]. Paolo Mercorelli and Nils Werner utilized adaptive control strategy to deal with the servo valve resonance problem. Experimental results showed that adaptive resonance regulator can adaptively change in accordance with any change

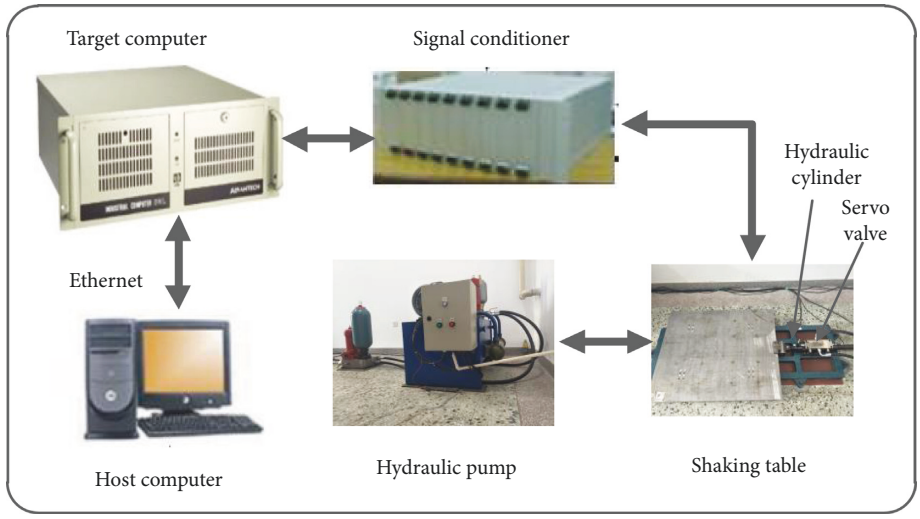

Figure 1: The hydraulic servo shaking table system.

in the velocity of the revolution of the engine [16]. Wang et al. adopted the modified resonance frequency detection and reduction method based on an adaptive notch filter to extend the middle frequency range of an industrial servo system [17]. Wang et al. presented an improved adaptive filtered x-LMS algorithm to suppress the resonance in the elastic drive system, which proves the better resonance suppression effect as well as convergence speed than the conventional method [18]. Rahman put forward a discrete time adaptive compensator based on an autotuning algorithm to suppress the time-varying resonance characteristics of a hard drive servo system [19]. Wang et al. proposed a model predictive control method to suppress mechanical resonance of a two-mass servo system; in addition, amplitude limit of the shaft torque dynamic performance was improved [20]. Yan et al. proposed an add-on multirate adaptive control scheme, which was based on a polynomial transformation technique and recursive least-squares algorithm, to compensate the uncertain resonance modes beyond the Nyquist frequency in high-performance mechatronic systems, and the vibration attenuation for uncertain resonances was effectively improved [21]. Besides, fuzzy control, robust control, and neural network were also presented to suppress the resonance modes of system whose resonance frequency varies frequently [22].

From the above literature, it is easy to find that the resonance suppression methods are mainly focused on mechanical system. As an integrated industrial equipment, the hydraulic servo shaking table needs to deal with electronic signal, hydraulic signal, and mechanical signal simultaneously, so accuracy and real time are highly required. Therefore, an adaptive notch filter based on LMS error principle is employed to identify the resonance frequencies online and real-time adjust the parameters of the notch filter. The output of resonance frequency detector which estimated all the resonance frequency components is injected into the adaptive notch filter to eliminate the appeared resonance modes. Simulation and experiment results validate the effectiveness of frequency identification and resonance suppression.

The rest of the paper is organized as follows. Section 2 first presents the hydraulic servo shaking table; afterwards, its control strategy and mathematical model are discussed. Section 3 introduces the adaptive notch filter design procedure and its theoretical analysis. The resonance suppression scheme is discussed in Section 4. Then, in section 5, simulation and experimental results are presented to validate the proposed method. Finally, the main points are concluded in section 6.

2. Hydraulic Servo Shaking Table System

Figure 1 shows the hydraulic servo shaking table system, which is a real-time operation system based on online rapid prototyping control technology xPC-Target. The host computer serves as the user interface and downloads the compiled program to the target computer by Ethernet adapter. The target computer converts voltage analog signal into current drive signal and performs real-time execution of compiled program. The hydraulic pump is used to provide hydraulic energy for shaking table and controls the pressure and flow of servo valve. The signal conditioner regulates the command signal and feedback signal to accurately reproduce the reference signal [23].

Figure 2 shows the control strategy of a hydraulic servo shaking table that mainly includes an input filter, servo valve, hydraulic cylinder, shaking table, and various transducers [24]. As the most common controller for the shaking table, the three variable controller (TVC) includes TVC feedforward controller and TVC feedback controller. The TVC feedback controller comprises of displacement, velocity, and acceleration feedback signals, where the displacement feedback signal is used to improve the closed-loop system stability, the velocity feedback signal is utilized to increase natural frequency of system, and the acceleration feedback signal is adopted to improve system's damping ratio. The displacement and acceleration feedback signal are measured

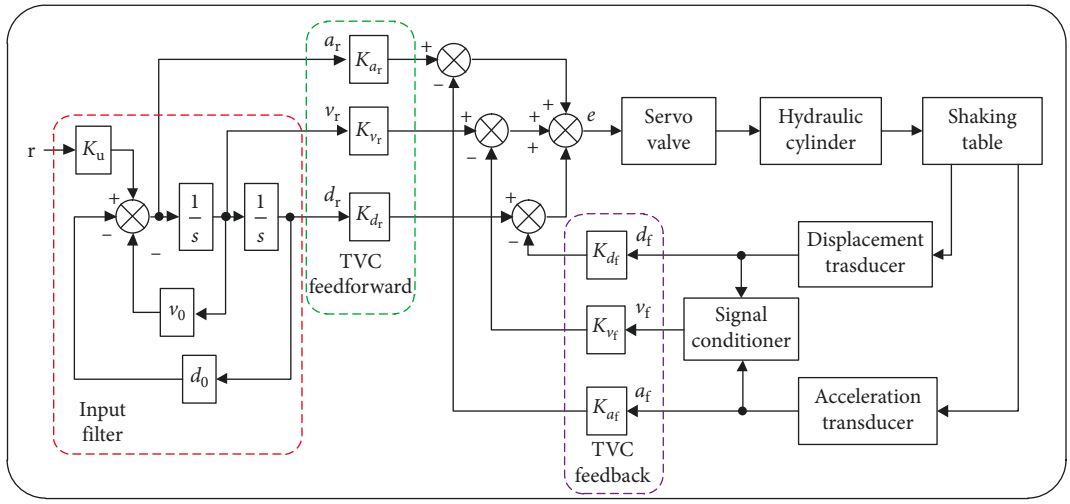

Figure 2: Control strategy of the hydraulic servo shaking table.

by displacement transducer and acceleration transducer, respectively. The velocity feedback signal is obtained from displacement feedback signal in low frequency range and acceleration feedback signal in high frequency range by signal conditioner because it is difficult to measure the three feedback signals simultaneously. The TVC feedforward controller including displacement, velocity, and acceleration feedforward signals generated by the input filter is mainly used to extend frequency bandwidth and reduce the tracking error. The error signal, which is the difference between reference signal and feedback signal, drives the hydraulic cylinder generating desired movement by servo valve [25].

The TVC control strategy is based on closed-loop position design, but the shaking table requires acceleration control. So, the reference displacement, velocity, and acceleration signals are obtained by the input filter [26]. The transfer function from input acceleration signal to displacement output signal can be deduced as

$$G_{re} = \frac{d_r}{r} = \frac{K_u}{s^2 + v_0 s + d_0} = \frac{K_u}{d_0\left(\left(s^2/\omega_0^2\right) + \left(2\zeta_0/\omega_0\right)s + 1\right)}, \tag{1}$$

where $d_0 = \omega_0^2$, $v_0 = 2\zeta_0\omega_0$, r is the reference acceleration, K_u is the acceleration gain, $\omega_0 = 0.4$ is the stating frequency of acceleration control, and $\zeta_0 = 0.6$ is the system's damping ratio.

The transfer function of the TVC feedforward controller can be expressed as

$$G_r = K_{d_r} + K_{v_r} s + K_{a_r} s^2, \tag{2}$$

where K_{a_r}, K_{v_r}, and K_{d_r} are corresponding acceleration, velocity, and displacement gain of feedforward controller. a_r, v_r, and d_r represent the reference acceleration, velocity, and displacement, respectively.

The transfer function of the TVC feedback controller can be described as

$$G_f = K_{d_f} + K_{v_f} s + K_{a_f} s^2, \tag{3}$$

where K_{a_f}, K_{v_f}, and K_{d_f} are feedback part's acceleration, velocity, and displacement. a_f, v_f, and d_f represent the measured acceleration, velocity, and displacement, respectively.

The servo valve regulates oil flow into the actuator chambers by changing the position of valve spool. The response of hydraulic oil flow Q to current control signal I can be approximated by the following second order transfer function

$$G_{sv}(s) = \frac{Q}{I} = \frac{K_{sv}}{\left(s^2/\omega_{sv}^2\right) + \left(2\zeta_{sv}/\omega_{sv}\right) + 1}, \tag{4}$$

where K_{sv}, ω_{sv}, and ζ_{sv} are gain, natural angular frequency, and damping coefficient of the servo valve.

The schematic diagram of hydraulic actuator controlled by servo valve is shown in Figure 3, where the specimen is simplified into a spring-mass-damping system. For convenience, p_s and p_o are supply and return pressure, q_1 and q_2 are input and output flow, p_1 and p_2 are input and output pressure, V_1 and V_2 are input and output oil volume, C_i and C_e are internal leakage and external leakage coefficient, m is the mass of the actuator, m_s is the mass of the specimen, x_v is the valve position, B is the viscous damping coefficient of the specimen, K is the spring stiffness of the specimen, A is the effective area of the piston, x_p is the displacement of the actuator, x_s is the displacement of the specimen.

The flow rate equation of the servo valve can be expressed as

$$q_L = K_q x_v - K_c p_L, \tag{5}$$

where $q_L = (q_1 + q_2)/2$ is load flow, $p_L = p_1 - p_2$ is load pressure, and K_q and K_c are flow gain and flow-pressure coefficient, which can be defined as

$$K_q = \frac{\partial q_L}{\partial x_v} = C_d W \sqrt{\frac{1}{\rho}(p_s - p_L)},$$
$$K_c = -\frac{\partial q_L}{\partial p_L} = \frac{C_d W x_v}{2(p_s - p_L)} \sqrt{\frac{1}{\rho}(p_s - p_L)}, \tag{6}$$

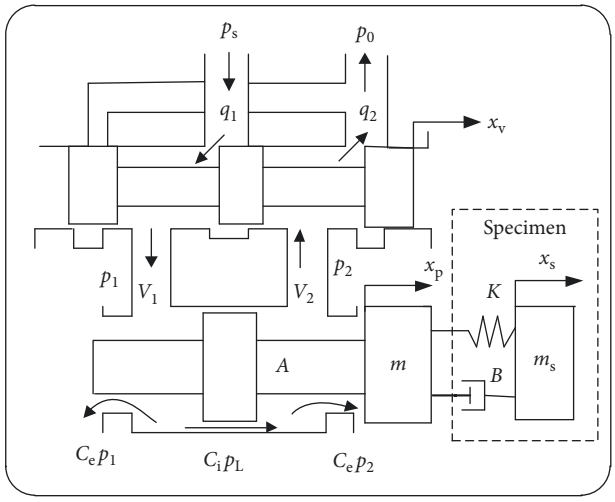

Figure 3: Schematic diagram of hydraulic actuator controlled by servo valve.

where C_d is flow coefficient, W is the gradient of valve orifices, and ρ is the density of hydraulic oil.

In consideration of oil elasticity, leakage, and chamber volume variation, the flow equation for each chamber can be formulated as

$$q_1 = A\frac{dx_p}{dt} + \frac{V_1}{\beta_e}\cdot\frac{dp_1}{dt} + C_i(p_1 - p_2) + C_e p_1, \tag{7}$$

$$q_2 = A\frac{dx_p}{dt} + C_i(p_1 - p_2) - \frac{V_2}{\beta_e}\cdot\frac{dp_2}{dt} - C_e p_2, \tag{8}$$

where β_e is the effective bulk modulus of hydraulic oil, $p_1 = (p_s + p_L)/2$, $p_2 = (p_s - p_L)/2$.

Combining equations (7) and (8) gives

$$q_L = A\frac{dx_p}{dt} + C_t p_L + \frac{V_t}{4\beta_e}\cdot\frac{dp_L}{dt}, \tag{9}$$

where $C_t = C_i + C_e/2$ is the total leakage coefficient and $V_t = V_1 + V_2$ is the total chamber volume.

Ignoring the oil mass and coulomb friction, the force balance equation of the shaking table and specimen can be expressed as

$$Ap_L = m\frac{d^2x_p}{dt^2} + B\left(\frac{dx_p}{dt} - \frac{dx_s}{dt}\right) + K\left(x_p - x_s\right), \tag{10}$$

$$K\left(x_p - x_s\right) + B\left(\frac{dx_p}{dt} - \frac{dx_s}{dt}\right) = m_s\frac{d^2x_s}{dt^2}. \tag{11}$$

Combining equations (5) and (9)–(11) and performing Laplace transform, the transfer function from the spool displacement to the displacement of hydraulic actuator can be derived as

$$G(s) = \frac{\left(K_q/A\right)\left(m_s s^2 + Bs + K\right)}{(mm_s/K_h)s^5 + [(B(m+m_s)/K_h) + (K_{ce}mm_s/A^2)]s^4 + [(K(m+m_s)/K_h) + (K_{ce}B(m+m_s)/A^2) + m_s]s^3 + [(KK_{ce}(m+m_s)/A^2) + B]s^2 + s}, \tag{12}$$

where $K_{ce} = K_c + C_t$ is the total pressure flow coefficient considering leakage. $K_h = 4\beta_e A^2/V_t$ is the hydraulic spring stiffness.

The specimen and shaking table itself form into resonance system due to the specimen's elastic load. The coupling term occurring in transfer function has a great influence on the specimen in the dynamic structure test of the hydraulic servo shaking table. Therefore, the adaptive notch filter must be designed to accommodate all the frequency variation.

3. Adaptive Notch Filter

The notch filter attenuates frequency characteristic to zero at center frequency while keeping the original value unchanged at other frequencies. However, the resonance frequency can vary due to various factors such as friction, dead zone, and manufacturing tolerances. The variation of resonance frequency may deteriorate the suppression performance of the notch filter. The notch filter with wider notch can attenuate to some extent the varying resonance mode. As the notch filter becomes wider, it also induces greater magnitude and phase lag at lower frequencies resulting in a lower bandwidth system. In order to solve the above problem, the adaptive notch filter whose center frequency varies online to track the resonance frequency is proposed to online real-time suppress the appeared resonance model.

The LMS algorithm is widely used in the adaptive filter due to its computational simplicity, unbiased convergence, and stable behavior. It is an iterative gradient descent algorithm that changes each iteration based on imperfect gradient estimate to seek the optimum value on the performance surface. The LMS algorithm can be written as follows [27, 28]:

$$\begin{cases} y_k = w_k^T x_k, \\ \varepsilon_k = d_k - y_k, \\ w_{k+1} = w_k + \alpha\varepsilon_k x_k, \end{cases} \tag{13}$$

where y_k is output signal, x_k is the reference input signal, w_k is the updating filter weight vector, d_k is the desired signal and ε_k is the error signal, and α denotes convergence factor that controls the stability and speed of adaptation. The signal propagation process from the reference input to the system output based on the LMS algorithm is shown in Figure 4 in detail.

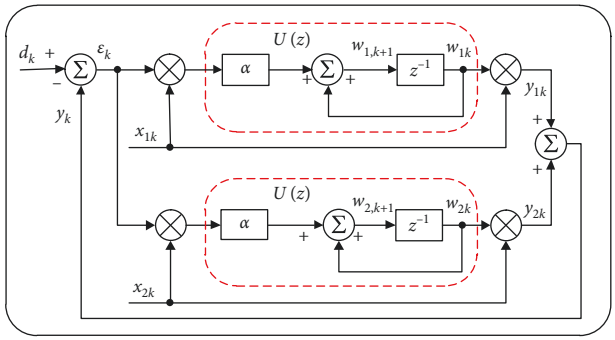

Figure 4: Flow diagram of the LMS adaptive algorithm.

The sampled reference inputs are

$$\begin{cases} x_{1k} = C\sin(\omega_r kT + \theta) = \dfrac{C\left[e^{j\omega_r kT}e^{j\theta} - e^{-j\omega_r kT}e^{-j\theta}\right]}{2j}, \\ x_{2k} = C\cos(\omega_r kT + \theta) = \dfrac{C\left[e^{j\omega_r kT}e^{j\theta} + e^{-j\omega_r kT}e^{-j\theta}\right]}{2}. \end{cases} \tag{14}$$

Following the path through the weight, we obtain

$$\begin{cases} Z[\varepsilon_k x_{1k}] = \dfrac{C\left[e^{j\theta}E(ze^{-j\omega_r T}) - e^{-j\theta}E(ze^{j\omega_r T})\right]}{2j}, \\ Z[\varepsilon_k x_{2k}] = \dfrac{C\left[e^{j\theta}E(ze^{-j\omega_r T}) + e^{-j\theta}E(ze^{j\omega_r T})\right]}{2}, \end{cases} \tag{15}$$

where $E(ze^{-j\omega_r T})$, $E(ze^{j\omega_r T})$ are $E(z)$ rotated counterclockwise and clockwise around the unit circle through an angle.

The weights are obtained as follows:

$$\begin{cases} W_1(z) = \dfrac{\alpha CU(z)\left[e^{j\theta}E(ze^{-j\omega_r T}) - e^{-j\theta}E(ze^{j\omega_r T})\right]}{2j}, \\ W_2(z) = \dfrac{\alpha CU(z)\left[e^{j\theta}E(ze^{-j\omega_r T}) + e^{-j\theta}E(ze^{j\omega_r T})\right]}{2}. \end{cases} \tag{16}$$

The contribution to the output at $Y(z)$ is

$$\begin{cases} Y_1(z) = \dfrac{C\left[e^{j\theta}w_1(ze^{-j\omega_r T}) - e^{-j\theta}w_1(ze^{j\omega_r T})\right]}{2j}, \\ Y_2(z) = \dfrac{C\left[e^{j\theta}w_2(ze^{-j\omega_r T}) + e^{-j\theta}w_1(ze^{j\omega_r T})\right]}{2}. \end{cases} \tag{17}$$

Combining equation (16) into equation (17), we obtain

$$Y(z) = \frac{\alpha CE(z)\left[U(ze^{-j\omega_r T}) + U(ze^{j\omega_r T})\right]}{2}. \tag{18}$$

The term in equation (18) represents the time invariant part of the response from $E(z)$ to $Y(z)$. The time invariant transfer function is

$$G(z) = \frac{Y(z)}{E(z)} = \frac{\alpha C^2(z\cos\omega_r T - 1)}{z^2 - 2z\cos\omega_r T + 1}, \tag{19}$$

where $G(z)$ has poles on the unit circle at $z = e^{\pm j\omega_r T}$, and a zero at $z = 1/\cos(\omega_r T)$.

The transform function from d_k to ε_k can be expressed as

$$G_{\text{notch}}(z) = \frac{E(z)}{D(z)} = \frac{z^2 - 2z\cos\omega_r T + 1}{z^2 - 2(1 - \alpha C^2/2)z\cos\omega_r T + 1 - \alpha C^2}. \tag{20}$$

For ease of exposition, equation (20) can be rewritten as follows:

$$G_{\text{notch}}(z) = \frac{\alpha_2 z^2 + \alpha_1 z + \alpha_0}{z^2 + \beta_1 z + \beta_0}. \tag{21}$$

The coefficients of the above adaptive notch filter are defined as [29]

$$\begin{cases} \alpha_2 = \dfrac{1 + 2\xi a\Omega_c + \Omega_c^2}{1 + 2\xi\Omega_c + \Omega_c^2}, \\ \alpha_1 = \dfrac{2(\Omega_c^2 - 1)}{1 + 2\xi\Omega_c + \Omega_c^2}, \\ \alpha_0 = \dfrac{1 - 2\xi a\Omega_c + \Omega_c^2}{1 + 2\xi\Omega_c + \Omega_c^2}, \\ \beta_1 = \dfrac{2(\Omega_c^2 - 1)}{1 + 2\xi\Omega_c + \Omega_c^2}, \\ \beta_0 = \dfrac{1 - 2\xi\Omega_c + \Omega_c^2}{1 + 2\xi\Omega_c + \Omega_c^2}, \end{cases} \tag{22}$$

where ξ and a determine the width and depth of the notch filter, respectively and $\Omega_c = \tan(\omega_c T/2)$ is related to the center frequency ω_c.

Figure 5 illustrates the amplitude-phase characteristic of the notch filter for different parameters. It is easy to see that the adaptive notch filter has larger notch width but larger phase delay as the same time. The larger phase delay may affect the system stability. Thus, the notch width should be kept as narrow as possible for the servo control system. In order to effectively suppress the variation of resonance frequency, it is necessary to online adjust the parameters of the notch filter with the varying resonance modes.

4. Resonance Suppression Scheme

Inspired by adaptive noise reduction, which adds the sinusoidal harmonics with just the right amplitude and phase to the primary signal including a noise signal to cancel the noise component, a new resonance suppression scheme based on the adaptive notch filter is shown in Figure 6. It is generally known that the peak of the frequency response in magnitude reaches the maximum value at resonance frequency. The signal with various resonance frequency is used

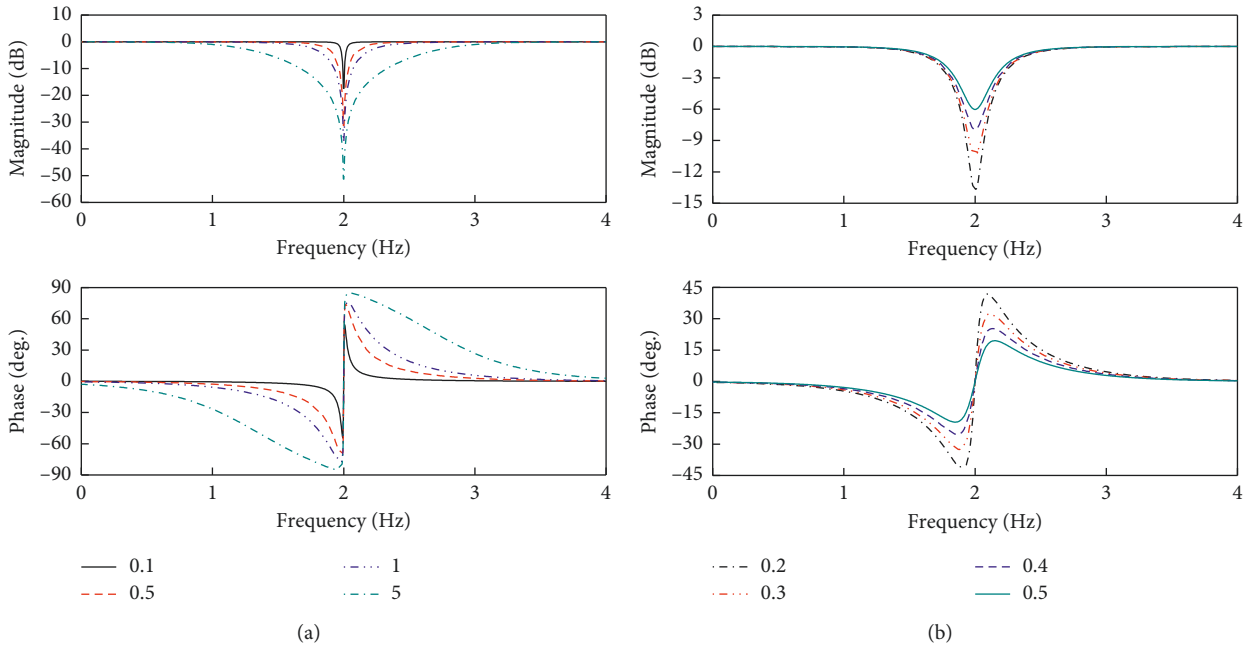

Figure 5: Bode diagram of the adaptive notch filter with different values. (a)a with constant and ξ with different values. (b)ξ with constant and a with different values.

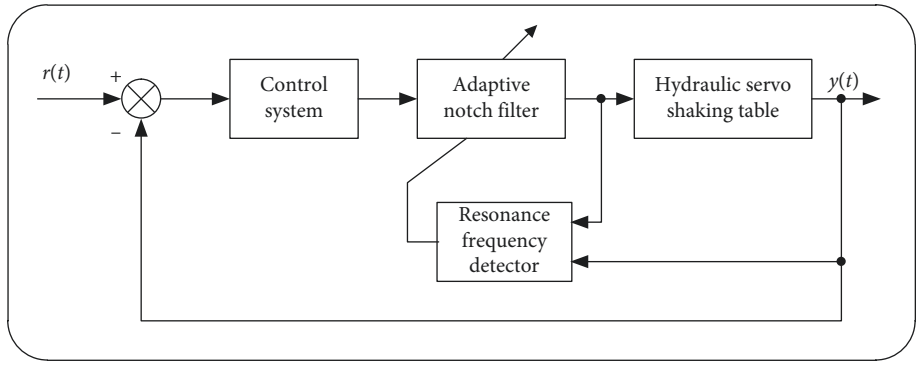

Figure 6: Schematic diagram of the resonance suppression.

as excitation signal to extract the resonance frequency component. Then, the resonance frequency is estimated by resonance frequency detector. With being placed in cascade between control system and hydraulic servo shaking table, the proposed adaptive notch filter can suppress the resonance modes with the variation of resonance frequency in real time.

The resonance frequency detector consists of an excitation signal generator and FIR filter. The excitation signal can be represented as

$$x_k^{\text{exc}} = \sum_{i=1}^{N} a_i \cos(\omega_i T k + \theta_i), \tag{23}$$

where ω_i denotes a group of resonance frequency candidates, which are spread around the actual resonance frequency. a_i and θ_i are the amplitude and phase of frequency components, respectively.

The transfer function of the FIR filter is given by

$$H(z) = 1 - 2\lambda z^{-1} + z^{-2}. \tag{24}$$

The frequency response of the FIR filter can be expressed by

$$\begin{aligned}\left|H\left(e^{j\omega T}\right)\right| &= \left|1 - 2\lambda e^{-j\omega T} + e^{-2j\omega T}\right| = \left|e^{-j\omega T}\right|\left|e^{j\omega T} - 2\lambda + e^{-j\omega T}\right| \\ &= 2|\cos(\omega T) - \lambda|.\end{aligned} \tag{25}$$

It is easy to see that the frequency is zero when $\lambda = \cos(\omega T)$ for $|\lambda| \le 1$. The amplitude of FIR filter output reaches the minimum value when the null frequency coincides with the frequency of the component having the largest amplitude among all the frequency components.

According to the linear system theory, the estimation output of the FIR filter is derived as

$$y_k = \sum_{i=1}^{N} a_i \left| H\left(e^{j\omega T}\right) \right| \cos\left(\omega_i T k + \theta_i + \angle H\left(e^{j\omega T}\right)\right). \quad (26)$$

The average power of the filter output signal y_k is defined as the objective function:

$$J = \frac{1}{L}\sum_{k=1}^{L} |y(k)|^2 = \frac{1}{2}\sum_{i=1}^{N} |a_i|^2 \left| H\left(e^{j\omega_i T}\right)\right|^2. \quad (27)$$

Substituting equation (25) into equation (27), the objective can be rewritten as

$$J = 2\sum_{i=1}^{N} |a_i|^2 |\cos(\omega_i T) - \lambda|^2. \quad (28)$$

It can be found that the objective function is a quadratic function of the filter coefficient λ. Taking the gradient of the objective function with respect to the filter coefficient and setting it equal to zero:

$$\frac{\partial J}{\partial \lambda} = 4\left[\sum_{i=1}^{N} |a_i|^2 \lambda - \sum_{i=1}^{N} |a_i|^2 \cos(\omega_i T)\right] = 0. \quad (29)$$

Thus, the optimal filter coefficient λ^* is found when the objective function reaches the minimization:

$$\lambda = \lambda^* = \frac{\sum_{i=1}^{N} |a_i|^2 \cos(\omega_i T)}{\sum_{i=1}^{N} |a_i|^2}. \quad (30)$$

Suppose that ω_r is the resonance frequency. Because the resonance frequency component has much larger amplitude than the other candidate components, the optimal coefficient λ^* in equation can be approximated as follows:

$$\begin{aligned} \lambda^* &= \frac{a_1^2 \cos(\omega_1 T) + a_2^2 \cos(\omega_2 T) + \cdots + a_N^2 \cos(\omega_N T)}{a_1^2 + a_2^2 + \cdots + a_N^2} \\ &= \frac{(a_1/a_r)^2 \cos(\omega_1 T) + (a_2/a_r)^2 \cos(\omega_2 T) + \cdots + (a_2/a_r)^2 \cos(\omega_N T)}{(a_1/a_r)^2 + (a_2/a_r)^2 + \cdots + (a_2/a_r)^2} \\ &\approx \cos(\omega_{re} T). \end{aligned} \quad (31)$$

The recursive algorithm for updating the filter coefficient can be described as

$$\lambda_{k+1} = \lambda_k + \frac{1}{2}\mu y_k x_{k-1}, \quad (32)$$

where μ is the adaptive gain.

$$\begin{aligned} \Omega_c^2 &= \left[\tan\left(\frac{\omega_c T}{2}\right)\right]^2 = \left[\tan\left(\frac{\omega_{re} T}{2}\right)\right]^2 \\ &= \frac{1 - \cos(\omega_{re} T)}{1 + \cos(\omega_{re} T)} = \frac{1 - \lambda^*}{1 + \lambda^*}. \end{aligned} \quad (33)$$

The optimal coefficients of the adaptive notch filter can be determined by

$$\begin{cases} \alpha_2^* = \dfrac{1 + \xi a\sqrt{1 - (\lambda^*)^2}}{1 + \xi\sqrt{1 - (\lambda^*)^2}}, \\ \alpha_1^* = \dfrac{-2\lambda^*}{1 + \xi\sqrt{1 - (\lambda^*)^2}}, \\ \alpha_0^* = \dfrac{1 - \xi a\sqrt{1 - (\lambda^*)^2}}{1 + \xi\sqrt{1 - (\lambda^*)^2}}, \\ \beta_1^* = \dfrac{-2\lambda^*}{1 + \xi\sqrt{1 - (\lambda^*)^2}}, \\ \beta_0^* = \dfrac{1 - \xi\sqrt{1 - (\lambda^*)^2}}{1 + \xi\sqrt{1 - (\lambda^*)^2}}. \end{cases} \quad (34)$$

5. Simulation and Experiment Results

5.1. Simulation Results. In this subsection, simulation is carried out to verify the effectiveness of the proposed adaptive notch filter for resonance suppression. The transfer function for simulation model consists of three resonance modes (39 Hz, 60 Hz, and 65 Hz), which is given by

$$G_s(s) = \frac{s^2 + 2 \times 0.01 \times (2\pi \times 60)s + (2\pi \times 60)^2}{\left[s^2 + 2 \times 0.035 \times (2\pi \times 39)s + (2\pi \times 39)^2\right]\left[s^2 + 2 \times 0.05 \times (2\pi \times 65)s + (2\pi \times 65)^2\right]}. \quad (35)$$

Figure 7 shows convergence of estimated frequency parameters. It can be seen that large fluctuation only occurred in initial stage, and frequency parameters quickly converge to reference value in a short time. This indicates that resonance frequency detector is able to estimate the resonance efficiently. The amplitude-phase characteristic of simulation with and without the adaptive notch filter is shown in Figure 8. It is clear that the system has three resonance frequencies, which severally restricts the dynamic performance and stability performance of system. However, the three resonance frequencies are significantly attenuated by the adaptive filter notch, compared with the case of the system without the adaptive notch filter. Although the bandwidth of shaking table is sacrificed, the stability of system is well ensured, which is important for shaking table test. The detailed parameters of the adaptive notch filter are listed in Table 1. This shows that the proposed adaptive notch filter is very effective in suppressing the resonance modes.

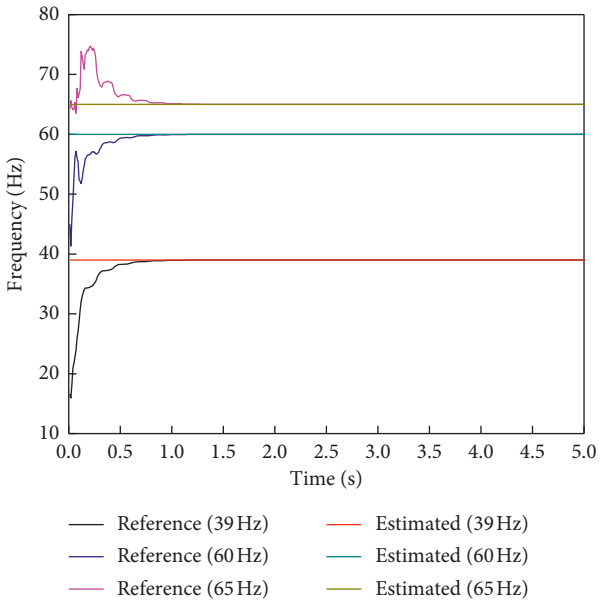

Figure 7: Convergence of estimated frequency parameters.

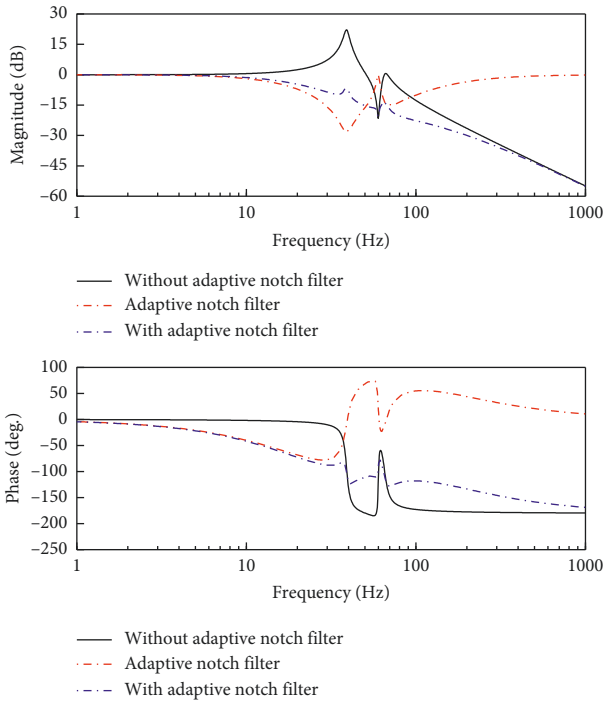

Figure 8: Amplitude-phase characteristic of simulation.

Figure 9 shows the sine sweep frequency response with and without the adaptive notch filter. As can be seen, magnitude at the resonance frequencies obviously decreases using the proposed method. Figure 10 shows the acceleration response of 3 $\sin(80\pi t)\text{m/s}^2$ excitation signal. It can be seen that the suppressed results have a good agreement with reference signal compared with unsuppressed results, which

Table 1: The parameters of adaptive notch filter.

	α_2^*	α_1^*	α_0^*	β_1^*	β_0^*
39 Hz	0.86	1.92	0.97	1.92	0.60
60 Hz	0.91	1.42	0.56	1.42	0.99
65 Hz	0.98	1.84	0.94	1.84	0.94

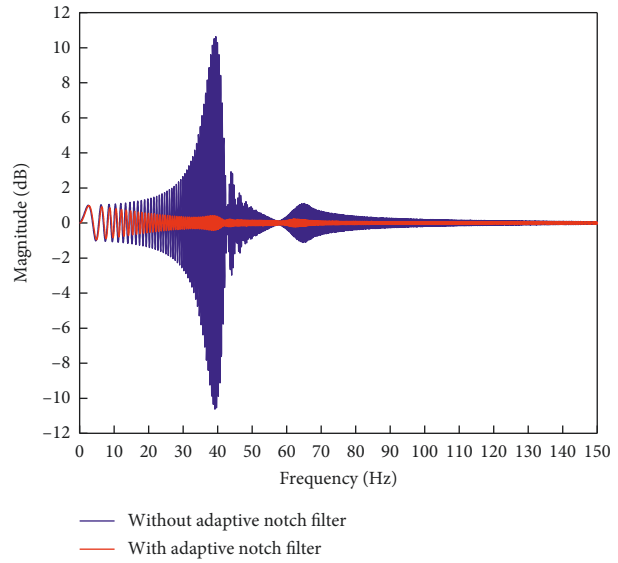

Figure 9: The sine sweep frequency response of simulation.

also proves that the proposed method has better performance on resonance suppression. Combined with the proposed adaptive notch filter, the final maximum tracking error is reduced from 1.8 m/s^2 to less than 0.1 m/s^2.

5.2. Experimental Results. The electrohydraulic servo shake table test used to validate the proposed resonance suppression scheme is shown in Figure 1, whose main parameters are listed in Table 2. The adaptive algorithm for the resonance frequency parameters estimation is depicted in Figure 11. Although there is an error at the beginning of the estimation process, the estimation of frequency is rapidly decreased and converges to steady state. Amplitude-phase characteristic of the shaking table system without the adaptive notch filter and with the adaptive notch filter is shown in Figure 12. The parameters calculation of the adaptive notch filter is similar with the simulation, not tried in words here. As can be seen, the generated three resonance modes are significantly attenuated using the proposed scheme. The gain margin and phase margin with the adaptive notch filter are greatly improved compared to without the adaptive notch filter, which is conductive to precise control of the hydraulic shaking table. The power spectrum of the response signal with and without the adaptive notch filter is shown in Figure 13. It is clear that amplitudes of the response signal are significantly attenuated

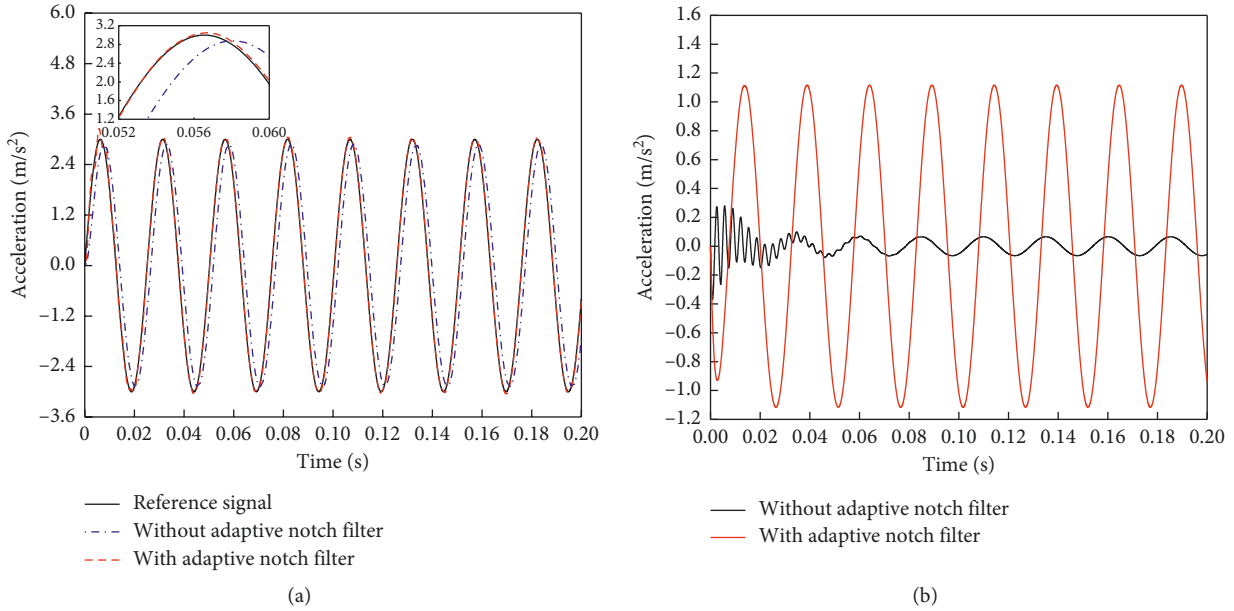

Figure 10: Sine acceleration response. (a) Tracking performance. (b) Tracking error.

Table 2: Main parameters of the hydraulic shaking table.

Parameters	Values
Flow gain K_q	2×10^{-3} m^3/s/A
Flow-pressure coefficient K_c	3×10^{-12} m^3/s/Pa
Piston's effective area A	1.9×10^{-3} m^2
Total leakage coefficient C_t	9×10^{-17} m^3/s/Pa
Total chamber volume V_t	3.78×10^{-4} m^3
Bulk modulus β_e	6.9×10^8 Pa
Viscous damping coefficient B	3.2×10^3 N/(m/s)
Spring stiffness K	1.7×10^6 N/m

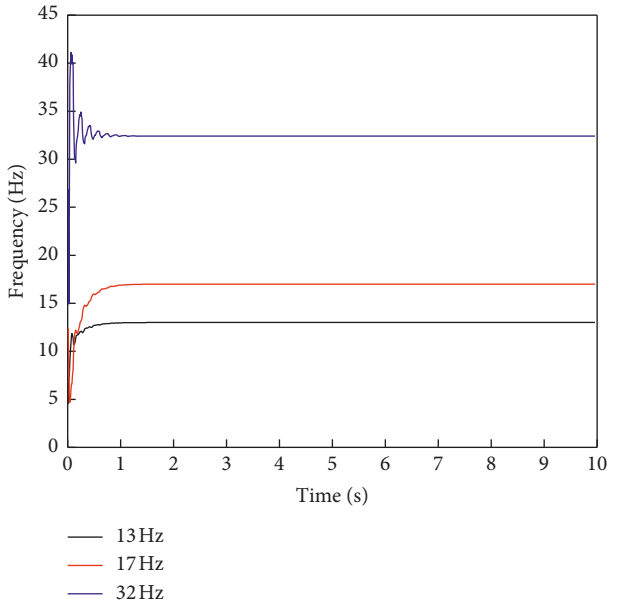

Figure 11: Convergence of estimated frequency parameters.

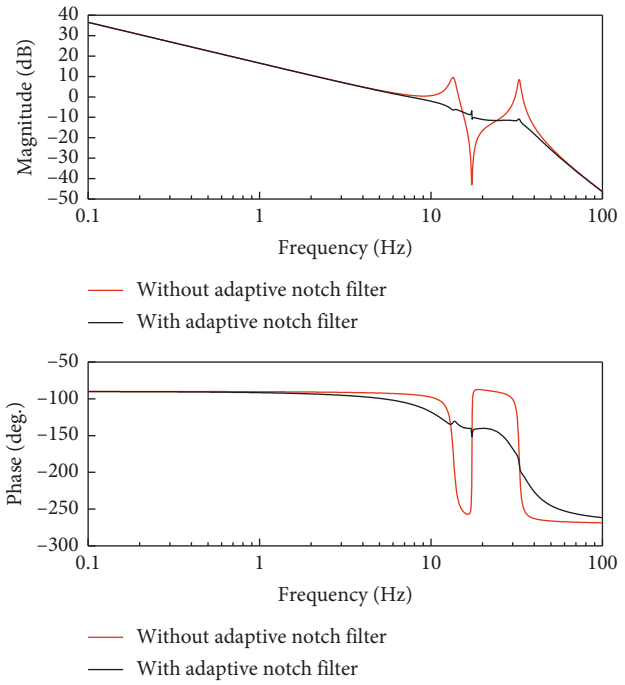

Figure 12: Amplitude-phase characteristic of shaking table system.

at the resonance frequency by using the proposed resonance suppression scheme.

Figure 14 shows the sine acceleration response of tracking performance and the tracking error with and without adaptive notch filter, where the excitation signal is $3 \sin(6\pi t)$m/s^2. It is obvious that sine acceleration response with the adaptive notch filter matches well with the reference signal compared with the situation without the adaptive notch filter. The tracking error of sine acceleration response

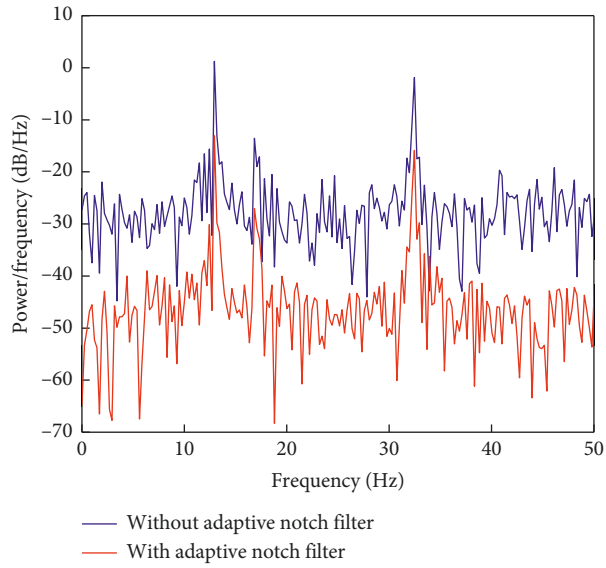

Figure 13: Experiment spectrum of response signal.

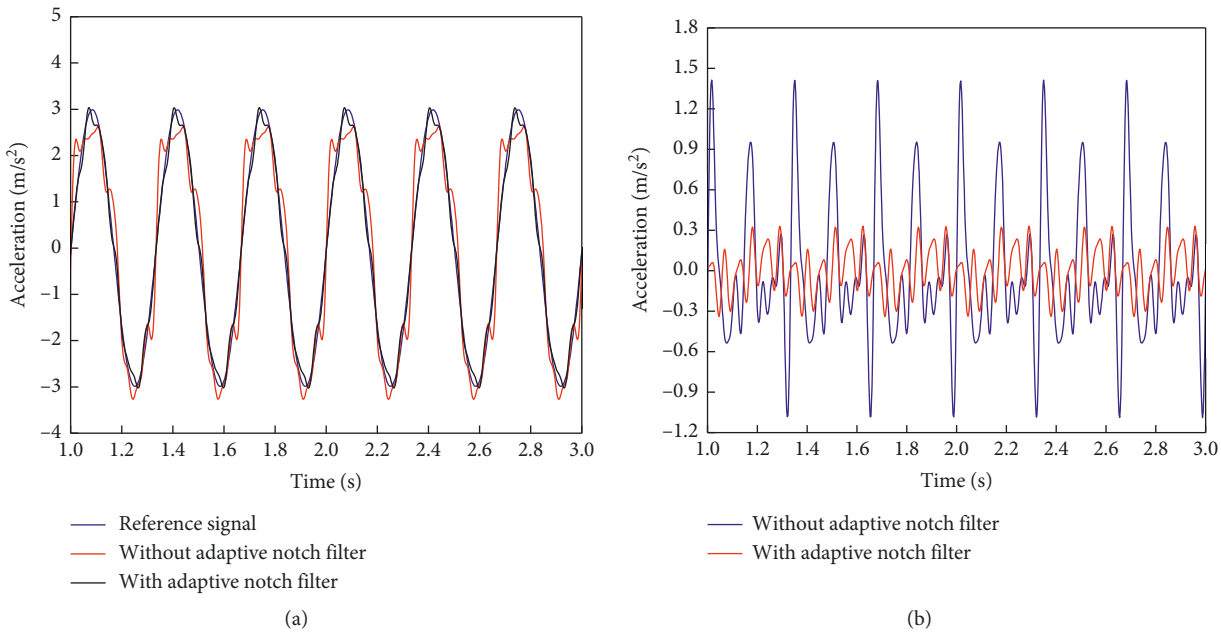

Figure 14: Sine acceleration response. (a) Tracking performance. (b) Tracking error.

reveals that the error has been greatly reduced by the adaptive notch filter from the initial maximum 1.5 m/s^2 to 0.3 m/s^2.

Apart from sine acceleration excitation signal, a recorded earthquake wave, which happened in El Centro in southern California, is also used to validate the proposed resonance suppression scheme. The experiment results of tracking performance and the tracking error are presented in Figure 15. As can be inferred from Figure 15, the proposed resonance suppression scheme with the adaptive notch filter has better tracking accuracy than without the adaptive notch filter.

6. Conclusions

In this paper, the operational principle and hydraulic actuator model are formulated to illustrate the resonance problem existing in the electrohydraulic servo shake table. The coupling between shaking table itself and the specimen's elastic load deteriorates the system's dynamic performance and even leads to the instability of the control system. Furthermore, the resonance frequency is a time-varying value during the shaking table test. In order to meet the requirements of resonance online suppressing, the

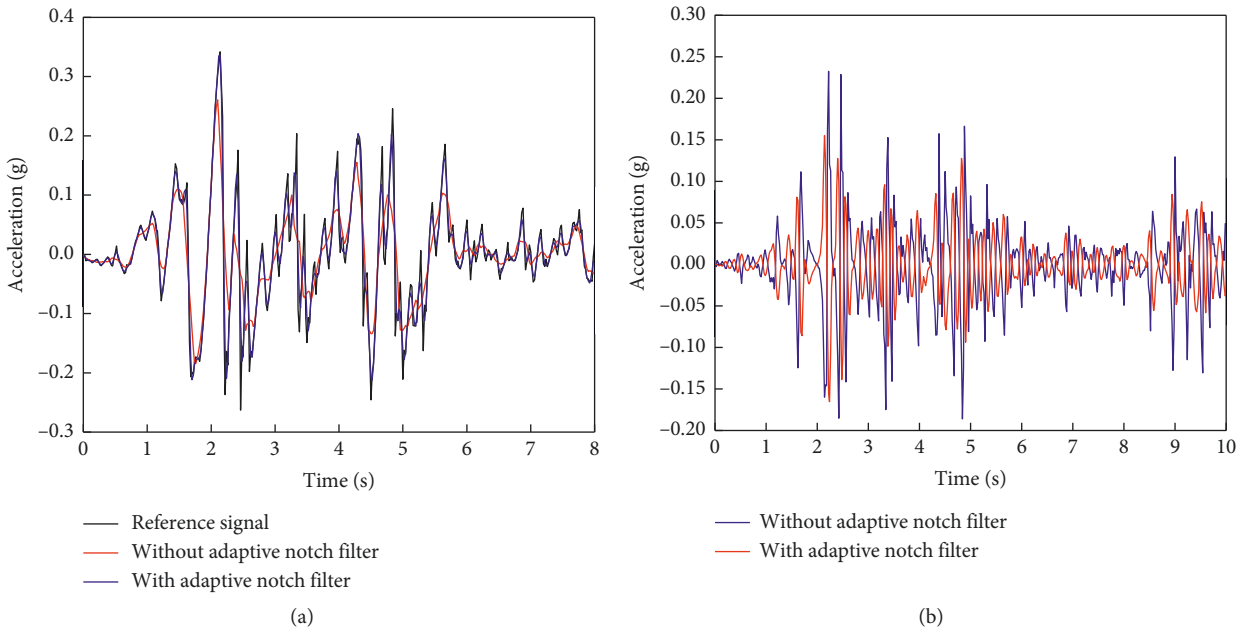

Figure 15: Experiment results of El Centro earthquake wave. (a) Tracking performance. (b) Tracking error.

adaptive notch filter based on the LMS adaptive algorithm is designed to online identify the resonance frequency and automatically adjust the filter coefficients. Simulation and experiment results demonstrate that the proposed method can be effectively used in suppressing the varying resonance mode.

Data Availability

The data used to support the findings of the study are available from the corresponding author upon request.

Conflicts of Interest

The authors declare no potential conflicts of interest with respect to the research, authorship, and/or publication of this article.

Acknowledgments

This project was supported by the Natural Science Foundation of Heilongjiang Province of China (grant no. E2018019) and the Fundamental Research Funds for the Central Universities (grant nos. HEUCFP201733 and HEUCFP201814).

References

[1] A. R. Plummer, "Special issue on control techniques for structural testing," *Proceedings of the Institution of Mechanical Engineers Part I-Journal of Systems and Control Engineering*, vol. 221, no. I2, pp. I–II, 2007.

[2] A. R. Plummer, "Model-based motion control for multi-axis servohydraulic shaking tables," *Control Engineering Practice*, vol. 53, pp. 109–122, 2016.

[3] J. Zhao, G. Shen, W. Zhu, C. Yang, and S. K. Agrawal, "Force tracking control of an electro-hydraulic control loading system on a flight simulator using inverse model control and a damping compensator," *Transactions of the Institute of Measurement and Control*, vol. 40, no. 1, pp. 135–147, 2018.

[4] G. Li, G. Shen, Z.-C. Zhu, X. Li, and W.-S. Zang, "Sine phase compensation combining an amplitude phase controller and a discrete feed-forward compensator for electro-hydraulic shaking tables," *Transactions of the Institute of Measurement and Control*, vol. 40, no. 11, pp. 3377–3389, 2018.

[5] Y. Tang, Z. Zhu, G. Shen, and W. Zhang, "Real time acceleration tracking of electro-hydraulic shake tables combining inverse compensation technique and neural-based adaptive controller," *IEEE Access*, vol. 5, pp. 23681–23694, 2017.

[6] J. J. Yao, G. L. Jiang, D. T. Di, and S. Liu, "Acceleration harmonic identification for an electro-hydraulic servo shaking table based on the normalized least-mean-square adaptive algorithm," *Journal of Vibration and Control*, vol. 19, no. 1, pp. 47–55, 2013.

[7] A. R. Plummer, "Control techniques for structural testing: a review," *Proceedings of the Institution of Mechanical Engineers Part I-Journal of Systems and Control Engineering*, vol. 221, no. I2, pp. 139–169, 2007.

[8] W. Kim, D. Won, D. Shin, and C. C. Chung, "Output feedback nonlinear control for electro-hydraulic systems," *Mechatronics*, vol. 22, no. 6, pp. 766–777, 2012.

[9] J. J. Yao, Z. S. Wan, and Y. Fu, "Acceleration harmonic estimation in a hydraulic shaking table using water cycle algorithm," *Shock and Vibration*, vol. 2018, Article ID 7278589, 12 pages, 2018.

[10] W. Shen, J.-z. Wang, and S.-k. Wang, "The control of the electro-hydraulic shaking table based on dynamic surface adaptive robust control," *Transactions of the Institute of Measurement and Control*, vol. 39, no. 8, pp. 1271–1280, 2017.

[11] R. Ghazali, Y. M. Sam, M. F. Rahmat, Z. Zulfatman, and A. W. I. M. Hashim, "Simulation and experimental studies on perfect tracking optimal control of an electrohydraulic

actuator system," *Journal of Control Science and Engineering*, vol. 2012, pp. 1–8, 2012.

[12] L. Zhang, D. Cong, Z. Yang, Y. Zhang, and J. Han, "Robust tracking and synchronization of double shaking tables based on adaptive sliding mode control with novel reaching law," *IEEE Access*, vol. 4, pp. 8686–8702, 2016.

[13] D.-H. Lee, J. H. Lee, and J.-W. Ahn, "Mechanical vibration reduction control of two-mass permanent magnet synchronous motor using adaptive notch filter with fast Fourier transform analysis," *IET Electric Power Applications*, vol. 6, no. 7, pp. 455–461, 2012.

[14] P. Schmidt and T. Rehm, "Notch filter tuning for resonant frequency reduction in dual inertia systems," in *Proceedings IEEE Industry Applications Society Annual Meeting*, Phoenix, AZ, USA, October 1999.

[15] Y. Wang, Q. Zheng, H. Zhang, and L. Miao, "Adaptive control and predictive control for torsional vibration suppression in helicopter/engine system," *IEEE Access*, vol. 6, pp. 23896–23906, 2018.

[16] P. Mercorelli and N. Werner, "An adaptive resonance regulator design for motion control of intake valves in camless engine systems," *IEEE Transactions on Industrial Electronics*, vol. 64, no. 4, pp. 3413–3422, 2017.

[17] W.-Y. Wang and A.-W. Shen, "Detection and reduction of middle-frequency resonance for industrial servo with self-tuning lowpass filter," *Journal of Control Science and Engineering*, vol. 2012, pp. 1–12, 2012.

[18] Y.-Q. Wang, F.-C. Huang, and H.-B. Liu, "Adaptive filtered x-least mean square algorithm with improved convergence for resonance suppression," *Proceedings of the Institution of Mechanical Engineers, Part I: Journal of Systems and Control Engineering*, vol. 228, no. 9, pp. 668–676, 2014.

[19] M. A. Rahman, A. A. Mamun, and K. Yao, "Discrete time adaptive controller for suppression of resonance in hard disk drive servo system," *International Journal of Control, Automation and Systems*, vol. 13, no. 5, pp. 1161–1172, 2015.

[20] C. Wang, M. Yang, G. Wang, and D. G. Xu, "IEEE, mechanical resonance suppression and shaft torque limitation of two-mass drive system based on model predictive control," in *Proceedings of the IECON 2014-40th Annual Conference of the IEEE Industrial Electronics Society*, pp. 2804–2809, Dallas, TX, USA, November 2014.

[21] W. Yan, C. Du, and C. K. Pang, "Multirate adaptive control of uncertain resonances beyond the Nyquist frequency in high-performance mechatronic systems," *Automatica*, vol. 66, pp. 63–72, 2016.

[22] T. Orlowska-Kowalska and K. Szabat, "Control of the drive system with stiff and elastic couplings using adaptive neuro-fuzzy approach," *IEEE Transactions on Industrial Electronics*, vol. 54, no. 1, pp. 228–240, 2007.

[23] J. Yao, H. Yan, R. Xiao et al., "Sinusoidal acceleration harmonic estimation using the extended Kalman filter for an electro-hydraulic servo shaking table," *Journal of Vibration and Control*, vol. 21, no. 8, pp. 1566–1579, 2015.

[24] K. Seki, M. Iwasaki, M. Kawafuku, H. Hirai, and K. Yasuda, "Adaptive compensation for reaction force with frequency variation in shaking table systems," *IEEE Transactions on Industrial Electronics*, vol. 56, no. 10, pp. 3864–3871, 2009.

[25] X. Li, Z. C. Zhu, G. C. Rui, D. Cheng, G. Shen, and Y. Tang, "Force loading tracking control of an electro-hydraulic actuator based on a nonlinear adaptive fuzzy backstepping control scheme," *Symmetry-Basel*, vol. 10, no. 5, 2018.

[26] J. Yao, D. Di, G. Jiang, S. Gao, and H. Yan, "Identification of acceleration harmonic for an electro-hydraulic servo shaking table based on Kalman filter," *Transactions of the Institute of Measurement and Control*, vol. 35, no. 8, pp. 986–996, 2013.

[27] J. Yao, D. Di, and J. Han, "Adaptive notch filter applied to acceleration harmonic cancellation of electro-hydraulic servo system," *Journal of Vibration and Control*, vol. 18, no. 5, pp. 641–650, 2012.

[28] J. Cadzow, "Digital notch filter design procedure," *IEEE Transactions on Acoustics Speech & Signal Processing*, vol. 22, no. 1, pp. 10–15, 2003.

[29] C. I. Kang and C. H. Kim, "An adaptive notch filter for suppressing mechanical resonance in high track density disk drives," *Microsystem Technologies*, vol. 11, no. 8-10, pp. 638–652, 2005.